Coupling of surface relaxation and polarization in $PbTiO_3$ from atomistic simulation

2008 J. Phys.: Condens. Matter 20 395004

(http://iopscience.iop.org/0953-8984/20/39/395004)

J. Phys.: Condens. Matter **20** (2008) 395004 (13pp) doi:10.1088/0953-8984/20/39/395004

Coupling of surface relaxation and polarization in $PbTiO_3$ from atomistic simulation

R K Behera[1], B B Hinojosa[2], S B Sinnott[1], A Asthagiri[2] and S R Phillpot[1,3]

[1] Department of Materials Science and Engineering, University of Florida, Gainesville, FL 32611, USA
[2] Department of Chemical Engineering, University of Florida, Gainesville, FL 32611, USA

E-mail: sphil@mse.ufl.edu

Received 27 June 2008, in final form 1 August 2008
Published 1 September 2008
Online at stacks.iop.org/JPhysCM/20/395004

Abstract

Molecular dynamics simulations are used to characterize ferroelectricity on the (001) surfaces of $PbTiO_3$ (PT), one of the most widely studied ferroelectric materials. Two different empirical interatomic shell model potentials are used. Both PbO and TiO_2 surface terminations in PT under open circuit electrical boundary conditions are characterized. The results are found to be in good agreement with the results of density functional theory calculations. The atomic relaxations, interlayer spacings and surface rumplings of each of the four possible surface terminations are analyzed. The deviation of the polarization from the bulk value is observed to be larger when the polarization points out of the surface than when it points into the surface. Analysis of the surface energies for free-standing films shows that polarization parallel to the surface is energetically more favorable than the polarization normal to the surfaces.

(Some figures in this article are in colour only in the electronic version)

1. Introduction

Epitaxially grown ultrathin films of ferroelectric materials, such as $BaTiO_3$ and $PbTiO_3$ (PT), have attracted considerable attention due to their numerous potential applications [1–3], including non-volatile memory components [4]. The relentless miniaturization of such electronic devices demands an atomic level understanding of their dielectric and ferroelectric properties. Surfaces are of particular interest, because they can be expected to have properties that are considerably different from those of the bulk.

Simulation is an ideal tool for probing ferroelectric phenomena because it can provide information with atomic and unit cell resolution that is not easily accessible from experiment. In particular, electronic-structure calculations at the level of density functional theory (DFT) can give extremely high-fidelity, material-specific information, and have been used with considerable success to study ferroelectric materials [5]. However, DFT is limited to relatively small system sizes, and generally to zero temperature. By contrast, while atomic level simulations based on classical interatomic potentials are more limited in their materials fidelity, they can be used to simulate significantly larger systems, thereby accessing microstructures not accessible to DFT. Moreover, they can easily incorporate non-zero temperatures and dynamical behavior in materials [6]. Indeed, atomistic simulation methods have been successfully used in ferroelectrics to study bulk properties [7, 8], solid solutions [9], superlattices [10], thin films [11], surfaces [12–14], and nanodots [15].

Here, we elucidate the structure and energetics of the (001) surfaces in PT under open circuit electrical boundary conditions. Previous simulations on ferroelectric thin films of PT [13, 14] have focused on the trends of the ferroelectric properties with system size. By contrast, here we are primarily concerned with the structure of individual surfaces. In addition, by comparing with the results of equivalent DFT calculations we also assess the ability of two different empirical interatomic potentials to describe such surface properties. As we shall see, the potentials can describe the surfaces quite well.

[3] Author to whom any correspondence should be addressed.

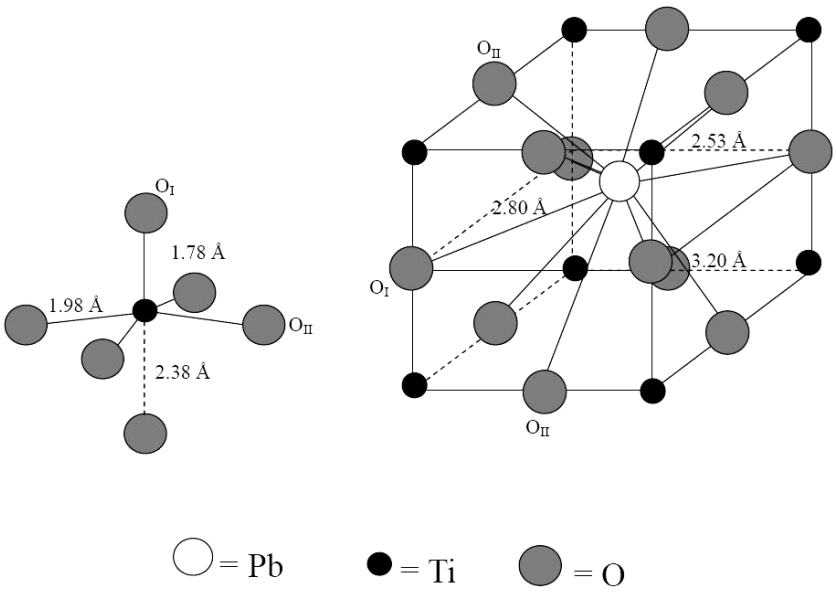

Figure 1. Schematic of tetragonal distortion of PT with Ti-environment and Pb-environment (adapted from [16]).

Table 1. Potential parameters used for describing short-range interactions [17, 18].

Atom	Core charge (e)	Shell charge (e)	k_2 (eV Å^{-2})	k_4 (eV Å^{-4})		A (eV)	ρ (Å)	C (eV Å^6)
				Potential 1				
Pb	+4.958	−2.785	119.48	17 968.5	Pb–Ti	0.096	2.420 131	−12.5665
Ti	+8.820	−5.158	1428.59	36 411.0	Pb–O	6766.270	0.273 805	127.7793
O	+0.563	−2.508	23.29	5 514.7	Ti–O	1130.010	0.359 723	−160.8363
					O–O	3634.861	0.314 424	331.6058
				Potential 2				
Pb	+5.1464	−3.3506	75.35	26 896.59	Pb–O	6291.337	0.265 259	296.2822
Ti	+9.7297	−6.8449	1937.88	961.16	Ti–O	1416.395	0.290 791	3.6840
O	+0.7057	−2.2659	26.48	1 324.55	O–O	283.410	0.520 557	−103.2676

2. Methodology

PT has the perovskite (ABO_3) structure with the Pb atoms occupying the cell corners, Ti occupying the body center, and the oxygen atoms sitting at the face centers. The cubic paraelectric phase has $Pm\bar{3}m$ symmetry, while the tetragonal ferroelectric phase has $P4mm$ symmetry. The bond lengths between the Pb–O and Ti–O ions in the room temperature ferroelectric structure are given in figure 1 [16].

We use two different shell model potentials, each parameterized to pertinent properties of PT. Potential 1, from Sepliarsky *et al* [17] and potential 2, from Asthagiri *et al* [18] differ in their description of the short-range interaction. In potential 1, the short-range interactions for the oxygen–oxygen (O–O) shells are described by the Buckingham potential,

$$V_{\text{Buck}}(r) = A\exp(-r/\rho) - C/r^6 \qquad (1)$$

where r is the separation between two ions, and A, ρ and C are free parameters. The Pb–Ti, Pb–O and Ti–O short-range interactions are described by the Rydberg potential:

$$V_{\text{Ryd}}(r) = (A + C^*r)\exp(-r/\rho) \qquad (2)$$

where again A, C and ρ are potential parameters. For potential 2, all of the short-ranged interactions are described by a Rydberg potential. For convenience, the parameters for both potentials are given in table 1. The cutoff distances used for potential 1 and potential 2 are 6.5 Å and 10.0 Å respectively.

A shell model is used with both potentials. In the shell model [19], each ion is described by a core and a shell, the sum of whose charges is the ionic charge, which is generally non-formal. The core and shell of each ion interact with the cores and shells of other ions via Coulombic interactions. In the traditional shell model, the core and shell of an atom are coupled by a harmonic spring. Both of these shell model potentials also include an anharmonic term in the core–shell interaction. The total core–shell interaction is given by:

$$V(\omega) = \tfrac{1}{2}k_2\omega^2 + \tfrac{1}{24}k_4\omega^4 + B(\omega-\omega_0)^2 \qquad \text{for } \omega > \omega_0, \quad (3)$$

where ω is the core–shell displacement, and k_2 and k_4 are the harmonic and anharmonic spring constants respectively. For potential 2, an additional core–shell penalty is implemented for each ion [7], for which $B = 250$ eV Å^{-2} and $\omega_0 = 0.2$ Å; for potential 1, $B = 0$. This penalty term ensures that the core–shell displacements remain within an acceptable range ($<\sim\omega_0$)

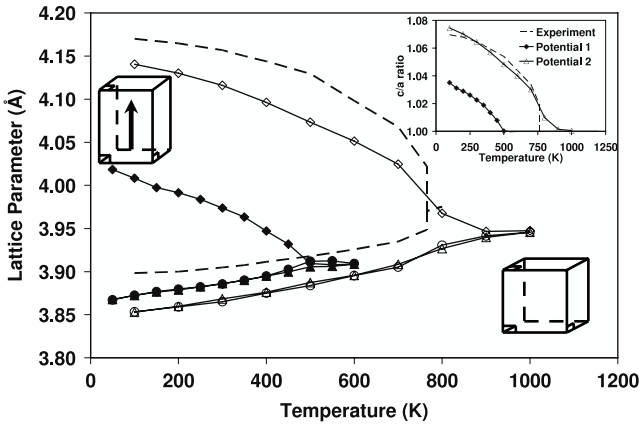

Figure 2. Lattice parameter as a function of temperature for PT. The experimental lattice parameter values are from [16, 25]. The lattice parameter for experiment, potential 1 and potential 2 are shown in dotted lines, solid lines with filled symbols and solid lines with open symbols respectively. Inset is the variation of c/a ratio compared with the experimental data.

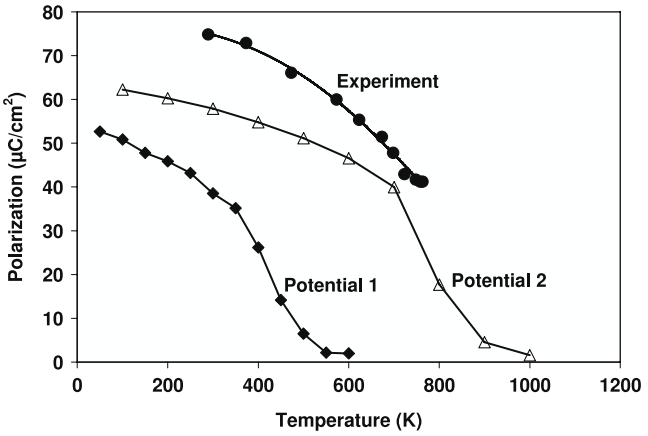

Figure 3. Polarization as a function of temperature for PT obtained with both the potentials. Experimental results are obtained from [27].

during the structural optimization. In all the systems studied here, the final core–shell displacement of each ion is less than ω_0. Even larger values of B have been used for potential 2 in a previous study [18].

In the MD codes used for these studies, the positions of the cores and shells are treated in a fully dynamic manner. In accord with previous use, in potential 1, the shells are assigned fictional masses of 10% of the mass of the individual ions. In potential 2, the shells are assigned a mass of 7 au for the cations and 2 au for the oxygen ions. The results obtained do not depend on these particular values.

In our atomistic simulations, the electrostatic forces are described by Coulombic interactions. The traditional approach to perform the conditionally convergent sums arising from the Coulomb interactions is the Ewald method [6, 20]. Although very powerful, the Ewald approach has a number of disadvantages. First, it is slow, with the computational load scaling as N^2, or at best $N \ln N$, where N is the total number of atoms. It also specifically requires that the system be three-dimensionally periodic. An extension of the Ewald method to two-dimensionally periodic systems has been made by Parry [21]; however, it is difficult to implement and scales even more prohibitively with system size. Here we use the direct summation method of Wolf *et al* [22], which is straightforward to implement, shows linear scaling independent of the periodicity of the system, and has been proven to be successful for the simulation of ferroelectric materials [10, 11, 23] and surfaces [13, 14].

As a baseline for the surface studies, the previously determined bulk properties of these potentials are reproduced. These simulations are performed on a $5 \times 5 \times 5$ unit cell system size (i.e., for 625 ions) with periodic boundary condition. The simulations are performed by solving Newton's equation of motion in an NPT ensemble with a 0.02 fs time step. A fifth order predictor–corrector algorithm is used to integrate the equation of motion. Velocity rescaling is used to maintain the temperature in the system [6]. The calculated effect of temperature on lattice parameter in bulk PT is shown in figure 2. As was seen previously [7, 17], both interatomic descriptions predict the tetragonal to cubic phase transformation as the temperature is increased. The variation of lattice parameter and c/a ratio shows qualitative agreement with experimental results [16, 24, 25]. In addition, evaluation of the polarization within the bulk PT structure confirms that both potentials reproduce the ferroelectric to paraelectric phase transformation (figure 3). The polarizations given by these potentials are comparable to experimental values [25–27]. Potential 2 has also been shown to reproduce the elastic constants to within 20–30 GPa of the experimental values for tetragonal PT at 300 K [28].

Clearly potential 2 displays much better quantitative agreement with experiment than potential 1. This is to be expected since potential 2 was developed after potential 1 and included additional DFT-derived data on the tetragonal PT bulk structure in the fitting database. Nevertheless, the degree of agreement between potential 2 and experiment for bulk PT is somewhat fortuitous. It is well known that the local density approximation (LDA) underestimates the experimental equilibrium volume and therefore potentials derived from DFT usually underestimate transition temperatures [7, 13]. Potential 2 was fit to a DFT database containing both PT and $Pb(Mg_{1/3}Nb_{2/3})O_3$ (PMN) information and was designed to simulate the compositional phase diagram of $Pb(Mg_{1/3}Nb_{2/3})O_3$–$x PbTiO_3$ [7]. A side effect of the inclusion of PMN data was that the quality of the fit to the DFT data of PT was actually poorer, but in the case of potential 2 this error is in the direction of the experimental values, resulting in a more accurate potential than would be expected. Because the degree of fidelity of the description of the bulk is different for the two potentials, a comparison between results obtained with each will allow us to identify generic behavior that does not depend sensitively on the potential.

In addition to the empirical potentials, first-principles calculations using Vanderbilt-ultrasoft pseudopotentials [29] based on DFT at the level of LDA are used as benchmarks against which to compare the surface results. The

pseudopotential treats Pb 5d and Ti 3p states explicitly as valence states. All the calculations are performed with 395 eV (29 Ryd) cutoff energies. The accuracy of the pseudopotentials and the effect of cutoff energy on convergence for PT has already been previously established [30–32]. A $1 \times 1 \times 7.5$ unit cell system is considered for all the symmetric slabs (PbO–PbO and TiO_2–TiO_2), and a $1 \times 1 \times 8$ unit cell is considered for the asymmetric slab calculations. These result in 15 and 16 cation-oxygen layers along the z-direction for the symmetric and asymmetric slabs respectively. The surfaces are created by adding a three unit cell thick vacuum in the z-direction. A $6 \times 6 \times 1$ k-point Monkhorst–Pack [33] mesh is used. All the DFT calculations were performed with VASP [34–36]. Lattice parameters of $a = 3.86$ Å and $c/a = 1.05$, were obtained by optimizing the bulk tetragonal PT structure, and were used for all the subsequent DFT calculations.

The DFT method yields high material fidelity but is limited in the size of the system that can be treated. For the current study, it can predict the atomic displacements accurately for the bulk and surface PT for very thin films; it cannot, however, reach sufficient thickness for the properties at the center of the film to recover their perfect crystal values. Also, DFT cannot provide individual surface energies of the terminated ferroelectric surfaces, which is necessary for establishing the order of stability of the surfaces. Atomistic simulations, on the other hand, are capable of simulating large systems and can separate the individual surface energies of different surface terminations.

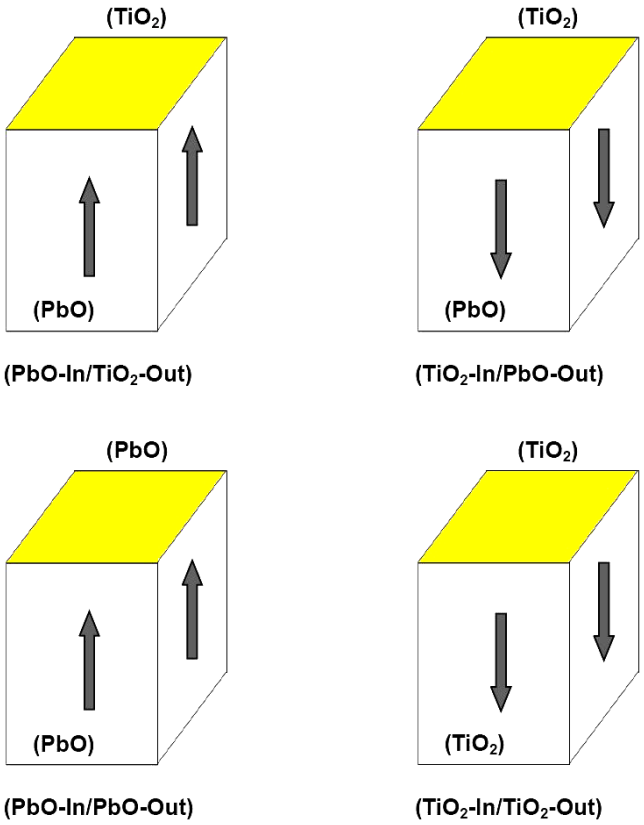

Figure 4. Schematic of all four possible free-standing ferroelectric films.

3. Surfaces

Free-standing films with (001) surface terminations are considered. The perovskite structure can form two distinct (001) surface terminations, exposing either a PbO layer or a TiO_2 layer. Based on the nominal valences of Pb^{2+}, Ti^{4+} and O^{2-}, both of these terminations are charge neutral. We consider films separately with TiO_2–TiO_2, TiO_2–PbO and PbO–PbO terminations. For a thin film system, when the ferroelectric polarization is perpendicular to the surface, one of the faces has polarization pointing into the film, while the other has polarization pointing out of the film. Polarization pointing into the surface is termed In-polarization, while polarization pointing out of the surface is termed Out-polarization. The direction of polarization depends on the relative displacement of the cations (Pb and Ti) with respect to the anions (O) in the unit cell. We discuss in detail below how In- and Out-polarizations are characterized at the atomic scale. The combination of different (001) surface terminations and the direction of polarization results in four possible configurations for free-standing films, as illustrated in figure 4. The asymmetric PbO-In/TiO_2-Out and TiO_2-In/PbO-Out structures are both formed by stoichiometric films. By contrast, the symmetric PbO-In/PbO-Out and TiO_2-In/TiO_2-Out structures are not stoichiometric. As we shall see, the surface structures and energies determined by MD simulation for each of the four distinct surfaces: PbO-In, PbO-Out, TiO_2-In and TiO_2-Out are independent of the type of surface on the other side of the film, strongly supporting our conclusion that this is a suitable simulation process for determining surface structures. Characterization of surfaces typically focuses on atomic relaxation, interlayer spacings, surface rumpling (shown schematically in figure 5) and surface energies. In the bulk, the ferroelectricity is associated with displacements of the atoms from their crystallographic sites (see figure 1), such that the Ti and O in a TiO_2 crystallographic plane, do not actually lie in a single physical plane. Similarly, the Pb and O in a PbO crystallographic plane do not lie in a single physical plane. Thus, to characterize the modifications of the crystal structure at the surfaces, the surface displacements of the ions are determined with respect to the positions they would have in a bulk terminated ferroelectric phase.

We simulate systems that are 6×6 unit cells in the x–y (001) plane and 32 unit cells thick (in the z-direction) which, as we shall see, is sufficiently thick for the middle layers of the film to have the properties of the bulk. All the surface simulations are performed at 0 K by relaxing all the ions (both cores and shells) in the system until all of the forces are less than 0.0001 eV $Å^{-1}$. To represent the effects of the presence of an infinitely thick film, the in-plane (x–y plane) lattice parameters are fixed to those of an ideal crystal in the ferroelectric phase, as described by each potential ($a = 3.866$ Å for potential 1 and $a = 3.843$ Å for potential 2).

Before examining the surface energetics and structure, it is important to assess the effects of the limitations of the atomistic methods. The most significant approximation of the empirical potentials used in this study, is that the charges on the ions

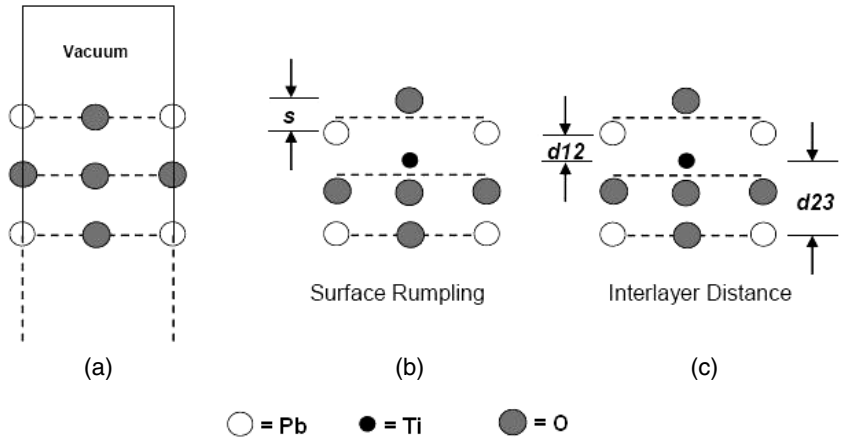

Figure 5. ⟨010⟩ view of (a) PbO-terminated PT with vacuum, (b) surface rumpling obtained after relaxation due to the movement of the individual atoms from the centro-symmetric position, and (c) change in the interlayer distance with the first two interlayers illustrated in the figure. The vacuum is not shown in (b) and (c) for clarity.

are fixed; there is thus no mechanism for the surface charges to be different from those of the bulk. To assess the impact of this approximation, we have performed a Bader charge analysis [37] for the PT surface determined from the DFT calculations. As shown in figure 6, the surface charges are only slightly different from the bulk values. An analysis of the Mulliken charges [38] on the PT surface also reported little charge difference with the bulk values. These small changes in the charges of atoms at the surface and compared with the bulk provide *a posteriori* justification for using fixed charge potentials for surface simulations.

Another important issue to address is the electrical boundary conditions for simulating ferroelectric thin films. There have been a number of DFT studies of 'short-circuit' boundary conditions [39–41] in symmetric slabs (i.e., PbO–PbO or TiO_2–TiO_2). This boundary condition has been achieved by (i) simulating the effects of metal electrodes, or (ii) by applying an external electric field in order to cancel the field inside the slab. In both cases, the idea is to reduce the effect of the depolarizing field created due to the difference in the charge distribution of the top and bottom surface of the ferroelectric slabs. Sai *et al* [40] and Kolpak *et al* [41] have examined the effect of Pt and $SrRuO_3$ electrodes on PT thin films. Pt electrodes are reported to stabilize the polarization in PT thin films by screening the depolarizing field, while $SrRuO_3$ electrodes partially compensate the surface charges, resulting in a polarization that is only half that of the bulk value in the interior of the thin film. Moreover, the presence of ferroelectricity depends on whether the structure of $SrRuO_3$ electrode is relaxed or not [40].

The application of an external electric field to compensate the depolarizing field was investigated by Mayer and Vanderbilt [39]. Though the application of this electric field led to reasonable $BaTiO_3$ thin film structures under short-circuit boundary conditions, the application of an electric field destroyed the ferroelectricity in PT. Given that there are significant unresolved technical issues associated with the short-circuit boundary conditions, even for electronic-structure calculations, we will focus on the 'open circuit' electrical boundary condition for our current thin film study.

Table 2. Surface characterization for PbO-terminations using DFT (in % of *c*-lattice parameter).

	PbO-In termination			PbO-Out termination		
Slab type	d_{12}	d_{23}	s	d_{12}	d_{23}	s
Symmetric	−4.00	0.01	5.31	−10.60	6.80	11.97
Asymmetric	−3.09	−0.27	4.37	−11.31	6.05	12.20

The 3D periodic unit cell contains an isolated, free-standing ferroelectric thin film with a vacuum region of 12 Å to prevent artificial interactions of one surface with the other through the periodic boundaries. Within this geometry, it is possible to examine both symmetric and asymmetric slabs. On one hand, the symmetric slabs (PbO–PbO and TiO_2–TiO_2) have no net dipole, but their non-stoichiometry can potentially influence the atomic displacements. On the other hand, asymmetric slabs are stoichiometric, but contain a dipole moment perpendicular to the slab due to the charged surfaces [38]. This dipole moment can lead to spurious dipole–dipole interactions in the direction normal to the surface due to the periodic boundary conditions. The dipole correction [42, 43] available in VASP for DFT calculations was used to correct for these interactions. In order to quantify the differences between symmetric and asymmetric slab configurations, we have performed DFT calculations with $1 \times 1 \times 7.5$ unit cells for symmetric slabs and $1 \times 1 \times 8$ unit cells for asymmetric slabs and characterized the surfaces (see tables 2 and 3). For all the terminations, the asymmetric and symmetric slab calculations show similar qualitative and semi-quantitative trends for surface structure. Using hybrid-DFT calculations, Piskunov *et al* [38] have reported comparable interlayer distances and surface rumpling for symmetric and asymmetric slabs in cubic PT. For sufficiently thick slabs, as we will show later in our MD simulations, the choice of symmetric versus asymmetric slabs does not affect the results.

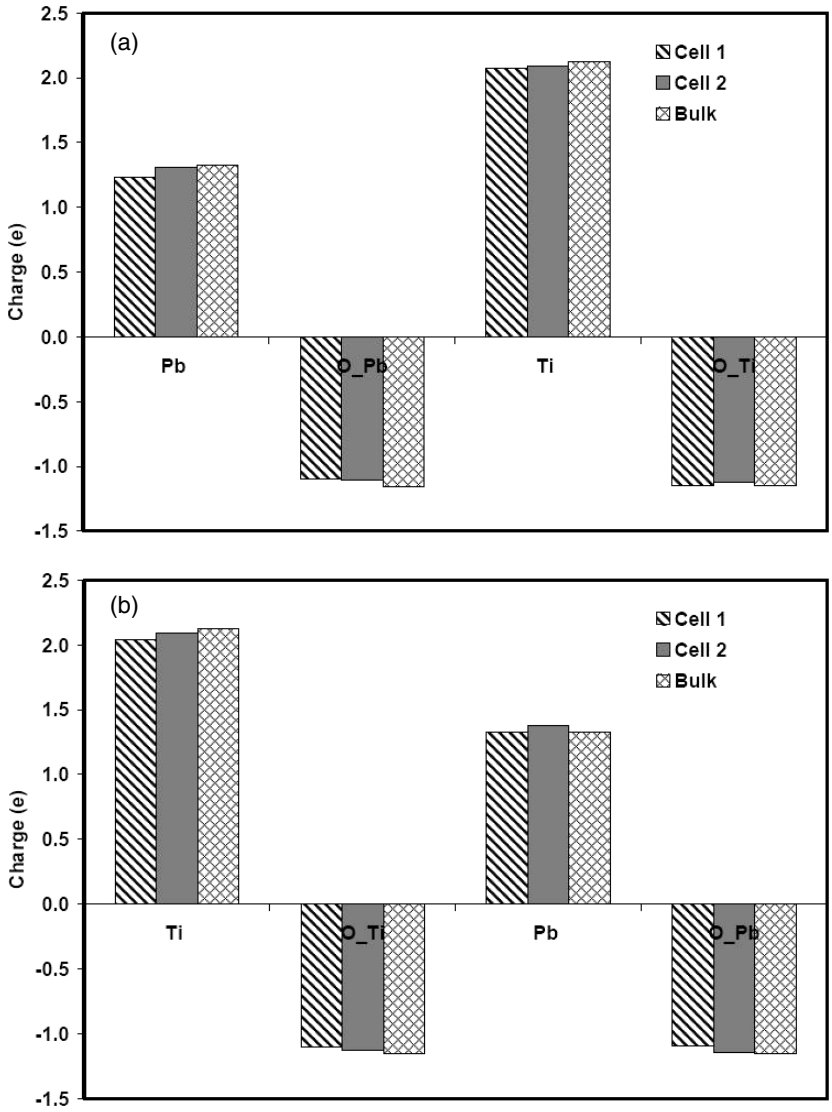

Figure 6. Comparison of the charge variation in each ion in surface and bulk with Bader charge analysis (a) PbO-terminated PT with vacuum, (b) TiO_2-terminated PT with vacuum. The maximum deviation (∼7%) is observed to be for the Pb-ions on the PbO-terminated surfaces. Similar result on charge variation is reported by Piskunov *et al* ([38]) with Mulliken charge analysis. Cell 1 and cell 2 represents the surface unit cell and the next sub-surface unit cell in the thin film, respectively.

Table 3. Surface characterizations for TiO_2-terminations using DFT (in % of *c*-lattice parameter).

	TiO_2-In termination			TiO_2-Out termination		
Slab type	d_{12}	d_{23}	s	d_{12}	d_{23}	s
Symmetric	−8.98	5.89	2.13	−6.70	2.38	10.75
Asymmetric	−8.60	5.74	2.06	−6.99	1.35	9.60

3.1. Surface structure

The atomic relaxation near the surface is calculated by examining the displacement of each ion from its equilibrium position in the bulk ferroelectric. Due to the planar symmetry of these films, the displacements of all the atoms of a single species are the same in each layer (i.e., each atomic x–y plane). The displacement of a metal ion and oxygen ion along the z-direction relative to the ferroelectric reference structure are given as $\delta_z(\mathrm{M})$ and $\delta_z(\mathrm{O})$ respectively. The interlayer distance (d_{ij}) is then defined as the difference between the cation displacements $\delta_z(\mathrm{M})$ between layer i and j. In particular, d_{12} is the cation spacing between the first (i.e., outermost) layer and the second layer, while d_{23} is the spacing between the second and third layers (see figure 5). For these calculations, the cations are taken as the reference because they scatter electrons more strongly than the oxygen ions, making them easier to detect experimentally [44]. We use the convention that a negative value corresponds to an inward displacement, while a positive value corresponds to an outward displacement. Rumpling is defined as the amplitude of relative displacements of the cations and oxygen in the same crystallographic plane, $s = |\delta_z(\mathrm{M}) - \delta_z(\mathrm{O})|$ [45]. For TiO_2 planes, an average displacement of the two oxygen atoms is considered for calculation.

Figures 7 and 8 illustrate the difference between the interlayer spacing in the outermost planes and the bulk value,

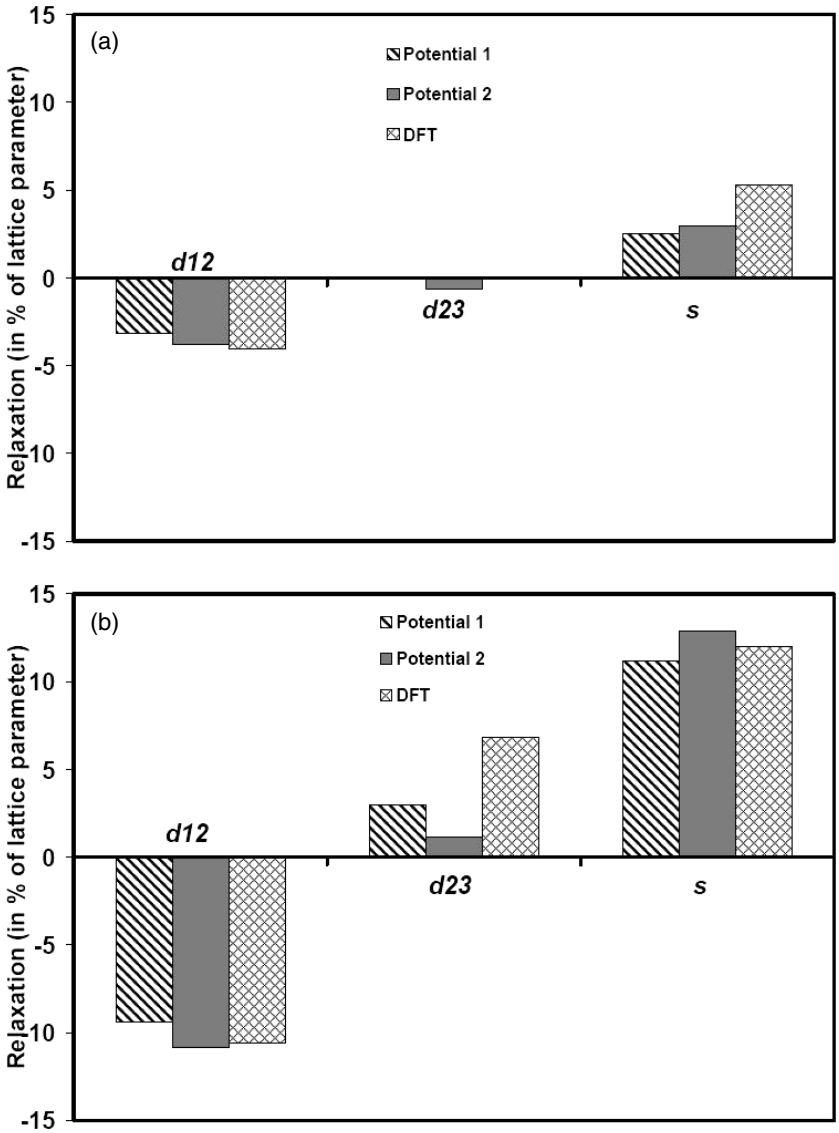

Figure 7. Interlayer distance and surface rumpling calculated for ferroelectric PT with surface, (a) PbO-In termination and (b) PbO-Out termination. The relaxation is given in per cent of c lattice parameter.

and the difference between the planar rumpling in the bulk and at the surface for both In- and Out-polarizations. For all four surfaces, both empirical potentials and the DFT calculations show that the surface relaxes inward, as evidenced by the negative values for d_{12}. Moreover, the predicted magnitude of the decrease is similar for the potentials and the DFT calculations. A similar level of agreement for the various methods also holds for the surface rumpling. The worst agreement is for d_{23}; however, in all cases d_{23} is rather small, and in only one case, TiO_2-Out termination, do the potentials predict an opposite sign from the DFT results. We conclude that the surface structures predicted by the potentials are qualitatively similar to DFT.

In order to analyze surface rumpling, the atomic displacement of individual cations and oxygens from bulk ferroelectric structure on each plane is calculated. Figure 9 shows all the surface atoms relax into the bulk for all surface terminations. For both terminations, the surface rumpling for Out-polarization surfaces are higher than the corresponding In-polarization cases. This is due to the larger cation displacement into the bulk compared to the oxygens for the Out-polarization surfaces (figures 9(b) and (d)) than the In-polarization surfaces (figures 9(a) and (c)).

3.2. Surface polarization

In addition to the structural details, the simulations provide valuable information on the change in polarization from the bulk to the surfaces of the films. The unit cell used for the calculation of the polarization depends on the nature of the surface. For TiO_2-terminated surfaces, a Pb-centered cell is analyzed; for PbO-terminated surfaces, a Ti-centered unit cell is analyzed. Because in the bulk-like interior of the film, the calculated value of the polarization is independent of the choice of a Ti-centered or Pb-centered unit cell, it is straightforward to determine the polarization in a physically sensible manner through the entire thickness of the film.

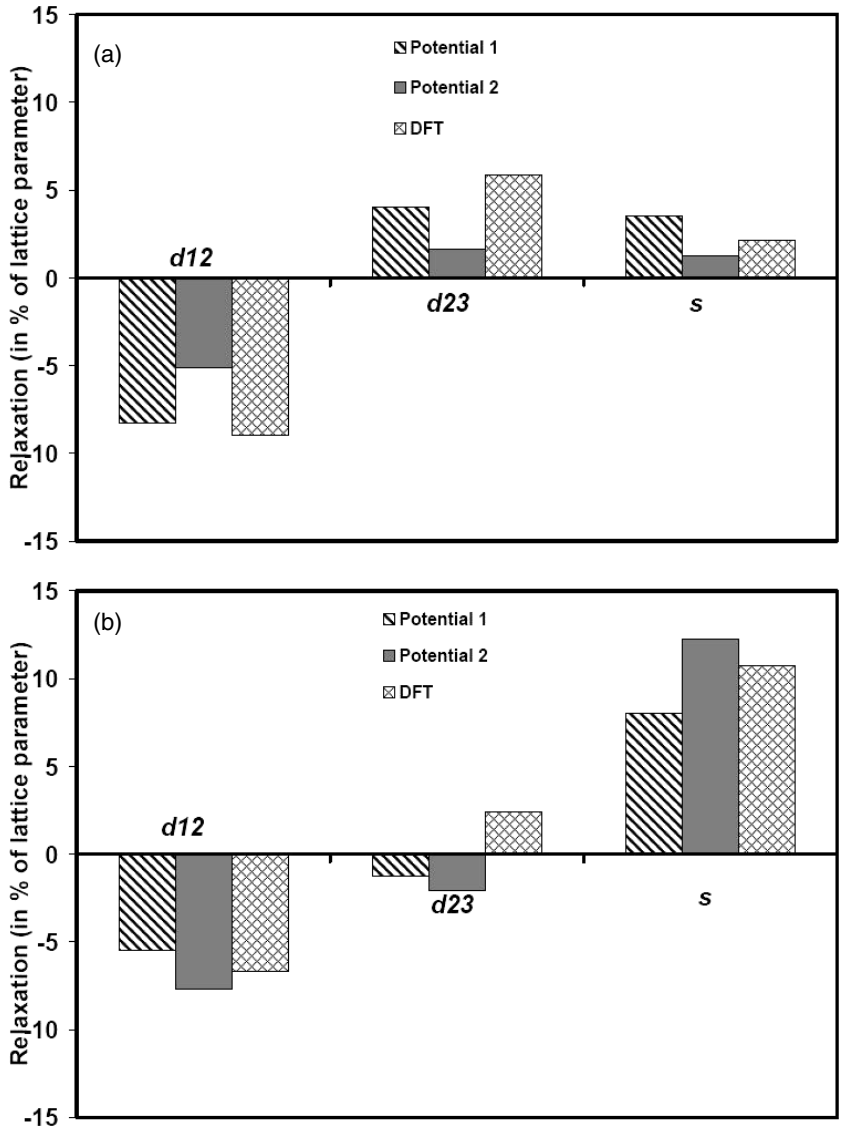

Figure 8. Interlayer distance and surface rumpling calculated for ferroelectric PT with surface, (a) TiO_2-In termination and (b) TiO_2-Out termination. The relaxation is given in per cent of c lattice parameter.

In order to further validate our empirical potential predictions, we calculate the cell-by-cell polarization for the DFT simulations. To do this we follow the method of Meyer and Vanderbilt [46]. We consider the final optimized output structure and the Born effective charges Z^*_α, for tetragonal PT, which we obtained from Zhong, King-Smith and Vanderbilt [47]. The polarization of each unit cell is then calculated as

$$P^{(i)} = \frac{e}{\Omega_c} \sum_\alpha w_\alpha Z^*_\alpha u^{(i)}_\alpha \tag{4}$$

where, e is the electron charge, Ω_C is the volume of one unit cell, u_α is the displacement of atom α from its centro-symmetric position, w_α is the corresponding weighting factor, corresponding to the number of atoms of that type in the unit cell. From the relaxed atomic position and the above expression, we obtained a bulk polarization of 81.0 μC cm^{-2}, which matches extremely well with the published value of 81.2 μC cm^{-2} [46].

To fully characterize the surface polarization, figure 10 provides a detailed profile, in unit cell thick slices, of the polarization normal to the PT thin film surfaces for thick films with PbO-Out/PbO-In and TiO_2-Out/TiO_2-In surfaces using potential 2. The results obtained from DFT calculations with a thinner film ($1 \times 1 \times 7.5$) are presented in the same plot for comparison, with the polarization of the four planes closest to the surface shown. The empirical potential results show that the polarization profile for each surface is independent of the type of surface (PbO or TiO_2) present on the other side of the film. For all of these relatively thick films, we see that the polarization in the interior of the film converges to the bulk single crystal values (60 μC cm^{-2} for potential 1 and 69 μC cm^{-2} for potential 2). However, for the films studied with DFT, the polarization in the center layer only reaches a value of $\sim$73 μC cm^{-2}, which is 10% less than the true bulk polarization. As illustrated in figure 10, the magnitude of the polarization is reduced at all of the surfaces, with

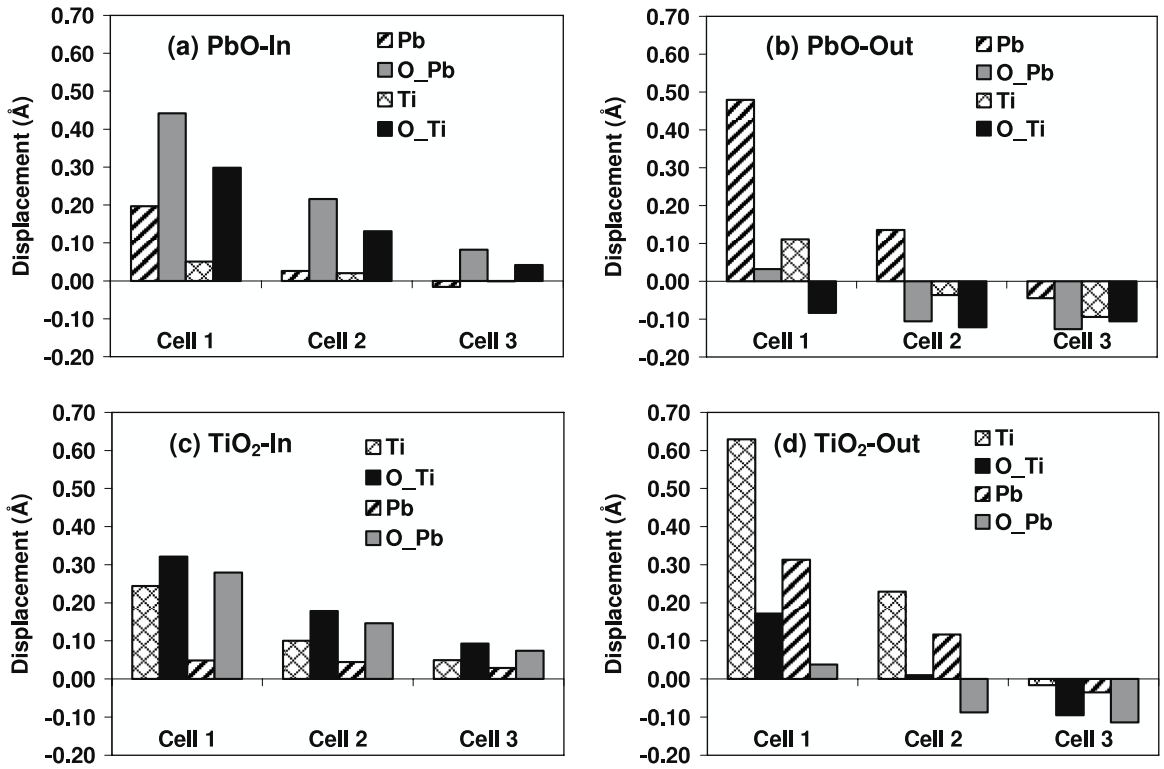

Figure 9. Cell-by-cell atomic displacement of each individual atom type from their original relaxed polarized condition with potential 2. (a) PbO-In, (b) PbO-Out, (c) TiO_2-In, and (d) TiO_2-Out surfaces. Cell 1, cell 2 and cell 3 represents the surface unit cell and the next two sub-surface unit cells in the thin film, respectively. Positive and negative values of displacement correspond to relaxation into and out of the surface, respectively.

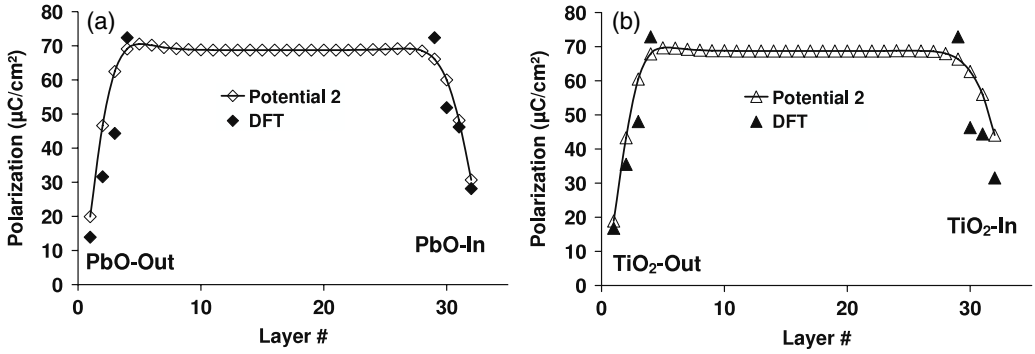

Figure 10. *c*-direction polarization obtained for a 6 × 6 × 32.5 tetragonal PT system with 10 units of vacuum in the c-direction with potential 2. Polarization variation in each unit cell perpendicular to the surface is reported where, (a) represents the polarization variation for PbO-Out/PbO-In and (b) represents the polarization variation for TiO_2-Out/TiO_2-In symmetric slabs. The 1 × 1 × 7.5 unit cell DFT results for respective terminations is presented as filled symbols in both the plots for comparison. Similar trend is observed for PbO-Out/TiO_2-In and TiO_2-Out/PbO-In terminations. The empirical potential results indicate that the films are thick enough to show bulk-like behavior in the middle of the film. The results indicate that the polarization in the Out-cases are lower compared to the corresponding In-cases, and for thick films it is independent of the surface termination on the other side of the film.

different surfaces showing decreases of different magnitudes. The polarization is more strongly suppressed for Out-than In-polarization cases, which is consistent with the first-principles prediction for PT thin films [39]. Similar results were observed for PbO-Out/TiO_2-In and TiO_2-Out/PbO-In surfaces. Simulations using potential 1 yield similar results.

The analysis of the surface polarization is made more complicated by the surface rumpling. Even for a conventional charge neutral ionic surface, such as the NaCl(001) surface, rumpling leads to a dipole moment in the surface region [48–50]. Although this rumpling leads to an electric polarization, it is of a qualitatively different nature from the ferroelectric polarization, since it is part of the inherent structure of the surface and, thus, cannot be switched by the application of an electric field. The presence of such a rumpling associated polarization at the PT(001) surface was seen previously by Sepliarsky *et al* [13] in the simulation of very thin films. In particular, they found that

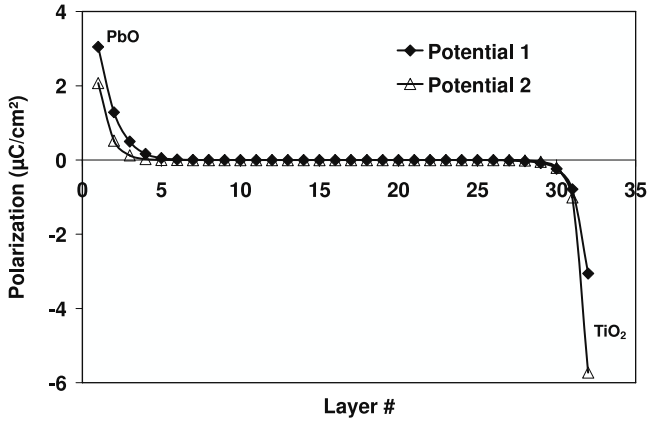

Figure 11. Polarization induced due to surface rumpling for tetragonal PT with no ferroelectricity for PbO-termination (left-hand side) and TiO_2-termination (right-hand side) with both the potentials. Positive values of polarization indicate total polarization along $+Z$ (into the surface, i.e., In-polarization for PbO-termination), while negative values indicate total polarization along $-Z$ (into the surface, i.e., In-polarization for TiO_2-termination).

for a four unit cell thick film, there was no polarization in the film interior. However, there was an inward polarization of $\sim 3\ \mu C\ cm^{-2}$ for PbO-terminated films. To estimate the effects of this rumpling for these films, we have simulated films with the in-plane lattice parameters of the ferroelectric phase, but with the shell model turned off, thereby suppressing the ferroelectricity. As shown in figure 11, this surface relaxation results in a polarization pointing into the film surface for both PbO and TiO_2 terminations, with magnitudes less than $10\ \mu C\ cm^{-2}$ for all surfaces. These inward polarizations due to the rumpling contribute to the total polarization in the surface regions in different ways, depending on the direction of the ferroelectric polarization in the film. For surfaces with an In-polarization, the polarization due to rumpling tends to reinforce the ferroelectric polarization; for Out-polarization surfaces, the polarization due to rumpling tends to counteract the ferroelectric polarization. Thus, the In-polarization surfaces are expected to show a smaller deviation of the polarization from the bulk values than the Out-polarization surfaces. This is exactly what we observe in figure 10.

3.3. Surface energy

The relative stability of a surface is measured by its energy. The surface energies for all possible surface terminations are calculated using both empirical potentials and DFT. For the empirical potential calculations, the surface energies are obtained by a direct comparison between simulations of bulk single crystals and systems with surfaces.

To calculate the surface energies using DFT, the procedure developed by Heifets *et al* is followed [51]. First, the cleavage energies for unrelaxed PbO-In/PbO-Out and TiO_2-In/TiO_2-Out termination are calculated. Since cleaving a PbO-Out surface simultaneously generates a TiO_2-In surface and, similarly, a PbO-In surface generates a TiO_2-Out surface, the relevant cleavage energy is distributed equally between the respective surfaces. Therefore, the cleavage energy can be given as [51]:

$$E_s^{(\mathrm{unrel})} = \tfrac{1}{4}\left[E_{\mathrm{slab}}^{(\mathrm{unrel})}(\mathrm{PbO}) + E_{\mathrm{slab}}^{(\mathrm{unrel})}(\mathrm{TiO_2}) - N E_{\mathrm{bulk}}\right] \quad (5)$$

where, $E_{\mathrm{slab}}^{(\mathrm{unrel})}(\mathrm{PbO})$, and $E_{\mathrm{slab}}^{(\mathrm{unrel})}(\mathrm{TiO_2})$, includes the unrelaxed In- and Out-polarization slab energies for PbO and TiO_2 respectively, E_{bulk} is the energy per bulk unit cell and N is the number of bulk cells. The relaxation energies for PbO (In- and Out-) and TiO_2 (In- and Out-) are calculated by comparing the relaxed and unrelaxed energies:

$$E_{\mathrm{rel}}(A) = \tfrac{1}{2}\left[E_{\mathrm{slab}}(A) - E_{\mathrm{slab}}^{(\mathrm{unrel})}(A)\right] \quad (6)$$

where A is either the PbO or TiO_2 terminated slab. The surface energy for each termination is then calculated as a sum of the cleavage and relaxation energies.

$$E_s(A) = E_s^{(\mathrm{unrel})} + E_{\mathrm{rel}}(A). \quad (7)$$

This surface energy for each termination represents the average energy of the In- and Out-polarization.

Figure 12 compares the average surface energies as calculated with the potentials and with DFT. In each case, it is seen that there is little difference between the PbO-In/PbO-Out average energy and the TiO_2-In/TiO_2-Out surface energies. Potential 2 and DFT predict similar average surface energies with opposite order of stability. However, since the differences are rather small this is not a major concern.

In their study of ultrathin films (fewer than 8 layers) using potential 1, Sepliarsky *et al* [13] observed an in-plane reconstruction that leads to a polarization parallel to ⟨110⟩, with an energy decrease of 0.002 eV/unit cell. This energy difference is significantly smaller than the energy differences between the In- and Out-polarization surfaces seen in this study, and thus we do not consider it here.

The DFT approach provides only the average energy for the In- and Out-polarization of a specific termination. However, our atomistic simulations can separate the individual surface energy contributions for the In- and Out-polarizations. In particular, as the inset to figure 13 shows, in the interior of the film the energy per unit cell converges to that for the bulk single crystal. It is thus straightforward to calculate the individual surface energies, by summing the excess energies layer by layer from the relevant surface to a region in the interior where the single crystal energy is recovered. The trends in the surface energies for each termination are the same for both potentials, as shown in figure 13. In particular, both potentials predict that Out-polarization surfaces are considerably lower in energy than the corresponding surface with In-polarization. While potential 1 predicts the TiO_2-Out surface to have a slightly lower energy, potential 2 predicts the PbO-Out surface to be more stable. Unfortunately, the DFT calculations cannot provide a definitive answer as to which is truly lower in energy, though the good agreement for the average energies shown in figure 12, gives the results for potential 2 significant credibility.

A key question is why the Out-polarization surface configuration is so much lower in energy than the In-polarization configuration. The answer to this lies in the

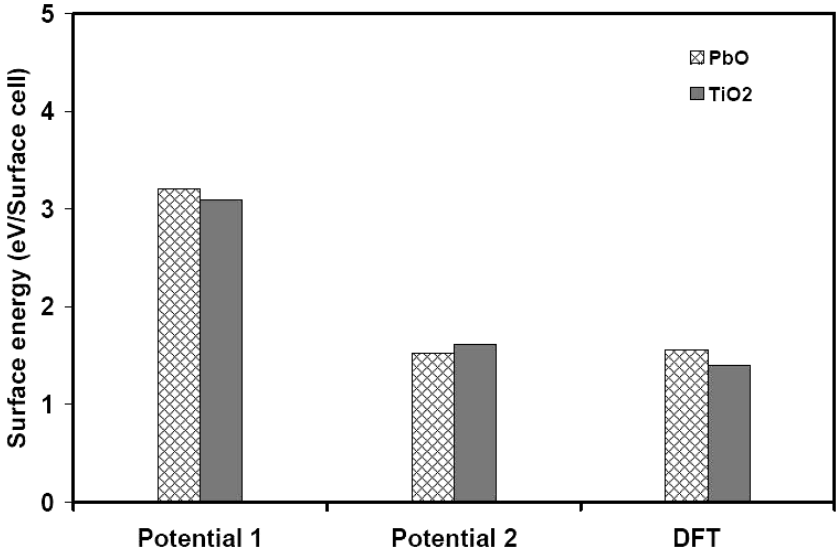

Figure 12. Comparison of average In- and Out-polarization surface energies for PbO- and TiO_2-termination in tetragonal PT.

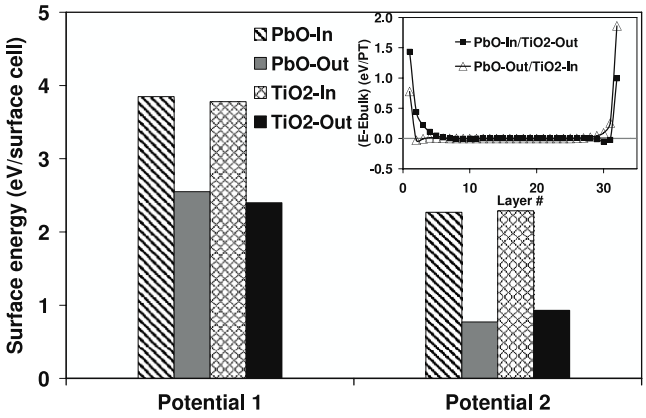

Figure 13. Individual In- and Out-polarization surface energies predicted from both the empirical potentials. Inset shows the excess energy per unit cell compared to bulk PT along the Z-direction for the PbO–TiO_2 surfaces with potential 2. Similar energy profile was obtained with potential 1. The excess energies are added to obtain the surface energy per surface cell for each termination.

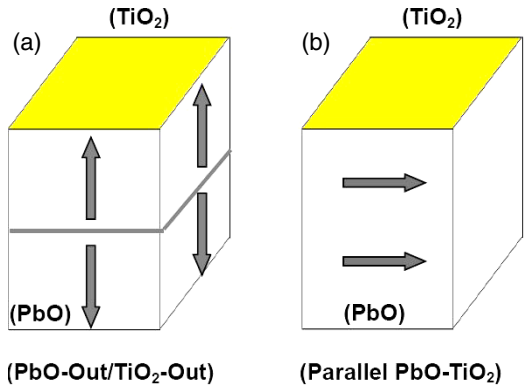

Figure 14. Schematic of (a) asymmetric Out–Out (tail–tail) polarization condition, and (b) asymmetric parallel polarization condition in free-standing ferroelectric films. For symmetric slabs the terminations on both sides will be either PbO or TiO_2, which are not shown here for clarity.

relative signs of the atomic displacements due to the surface rumpling and the polarization. As discussed above, the coupling of surface rumpling with surface relaxation in the ferroelectric films reduces the polarization in the Out-polarization surfaces more compared to the In-polarization surfaces for each termination. Also, the atomic relaxations indicate that the inward cation movement is more favorable in stabilizing the surfaces for the individual terminations compared to the inward oxygen movement at the surface.

3.4. Stability of free-standing thin films

By definition, a free-standing thin film has two free surfaces. From the discussion above, the PT system would strongly favor having the polarization pointing out of each surface. To support such a structure, the film would have to have an interface between an up and down domain running parallel to the surface. Physically, this is extremely unlikely, as it corresponds to dipole moments of opposite directions being end to end (see figure 14(a)). We have calculated the energy of such a domain wall and found it to be 2.02 and 2.28 eV/surface cell for potential 1 and 2 respectively. Thus the total energy required for two Out-polarization surfaces plus an interface is larger than that of the corresponding surface energies of the In-Out system.

This result does not, however, mean that the In-Out films are the most stable of all possible configurations in free-standing films. Another possibility is that the polarization in such systems does not lie normal to the film surface. We have performed simulations of films in which the polarization lies parallel to the surface (figure 14(b)) and find the sum of the surface energies for the PbO–TiO_2 surface terminations to be 5.32 and 2.49 eV/surface cell for potential 1 and 2 respectively, which are less than the corresponding In-Out conditions. Our DFT calculations also show that the parallel polarization

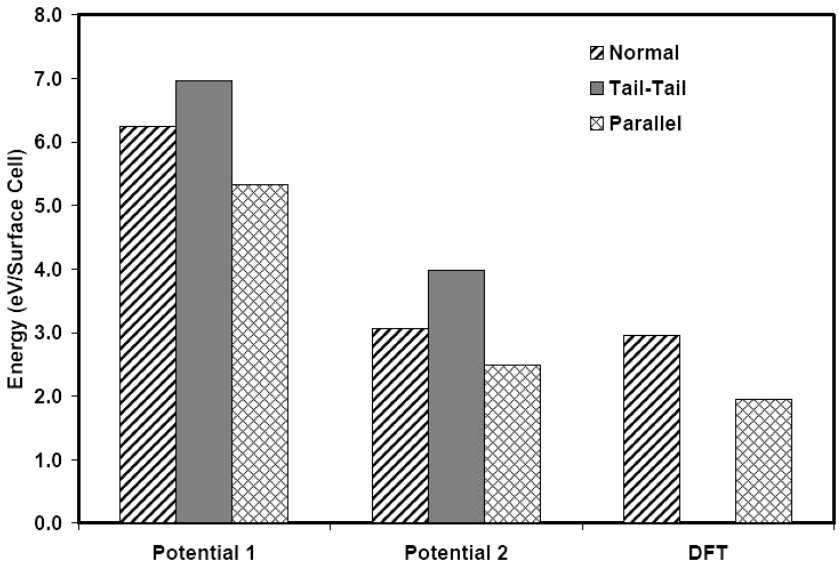

Figure 15. Total surface energy of PbO–TiO_2 terminated PT thin film for different termination-polarization combinations with empirical potentials and DFT simulations. Parallel polarization condition shows the lowest surface energy for all the simulations.

configuration is more stable than the In-Out configuration (figure 15). These calculations are consistent with previous DFT results for polarization parallel to the surface [45].

4. Discussion and conclusions

A key objective of this study was to assess the fidelity of these potentials for surfaces, as a prelude to an examination of the interaction of domain walls and surfaces. We conclude that both of these potentials lead to qualitatively similar results for the structure, polarization and energetics of these thin films, and that these results are consistent with DFT calculations. The surface characterizations predict that the Out-polarization surfaces are more stable than the In-polarization surfaces. However, for free-standing films under open circuit electrical boundary conditions, polarization parallel to the surface is observed to be more favorable. This gives us some confidence that the potentials can be used successfully to elucidate more complex behaviors in these materials.

The free-standing films considered here are a very special case. In most physical situations, these films are grown on a substrate. The presence of a substrate substantially modifies both the electrostatics of the system and the strain state, and consequently the stability of the system. The effect of the presence of a $SrTiO_3$ substrate has been extensively analyzed by Sepliarsky *et al* [14] using atomistic simulations.

A nanodot is an even more complex structure from the viewpoint of electrostatics. Indeed, Stachiotti [15] has explored the domain structure in nanodots in $BaTiO_3$ by reducing the lateral dimension of the cubic thin film. While the decrease in the lateral size does not decrease the ferroelectric properties of the thin film, the domain structure in the nanodot strongly depends on the type of surface termination. The Ti-terminated nanodots are reported to show a core polarization along the [111] direction. The Ba-terminated nanocells show a net zero polarization due to the development of domains with opposite polarizations.

Overall, atomic level simulations are very useful tools in understanding the complex surface termination and polarization effects in PT thin films. Indeed, the high materials fidelity of these opens up the possibility of using these atomic level simulations to study life size nanodevices for future applications.

Acknowledgments

This work was supported by the National Science Foundation under DMR-0426870. We thank the High Performance Computing (HPC), University of Florida for providing resources for the density functional theory calculations.

References

[1] Dimos D and Mueller C H 1998 *Annu. Rev. Mater. Sci.* **28** 397–419
[2] Polla D L and Francis L F 1998 *Annu. Rev. Mater. Sci.* **28** 563–97
[3] Scott J F 1998 *Annu. Rev. Mater. Sci.* **28** 79–100
[4] Auciello O, Scott J F and Ramesh R 1998 *Phys. Today* **51** 22–7
[5] Dawber M, Rabe K M and Scott J F 2005 *Rev. Mod. Phys.* **77** 1083–130
[6] Allen M P and Tildesley D J 2004 *Computer Simulation of Liquids* (Oxford: Oxford Science)
[7] Sepliarsky M, Wu Z, Asthagiri A and Cohen R E 2004 *Ferroelectrics* **301** 55–9
[8] Tinte S, Stachiotti M G, Sepliarsky M, Migoni R L and Rodriguez C O 1999 *J. Phys.: Condens. Matter* **11** 9679–90
[9] Sepliarsky M, Phillpot S R, Wolf D, Stachiotti M G and Migoni R L 2000 *Appl. Phys. Lett.* **76** 3986–8
[10] Sepliarsky M, Phillpot S R, Wolf D, Stachiotti M G and Migoni R L 2001 *J. Appl. Phys.* **90** 4509–19
[11] Sepliarsky M, Stachiotti M G and Migoni R L 2006 *Phys. Rev. Lett.* **96** 137603

[12] Tinte S and Stachiotti M G 2001 *Phys. Rev.* B **64** 235403
[13] Sepliarsky M, Stachiotti M G and Migoni R L 2005 *Phys. Rev.* B **72** 014110
[14] Sepliarsky M, Stachiotti M G and Migoni R L 2006 *Ferroelectrics* **335** 3–12
[15] Stachiotti M G 2004 *Appl. Phys. Lett.* **84** 251–3
[16] Shirane G, Pepinsky R and Frazer B C 1956 *Acta Crystallogr.* **9** 131–40
[17] Sepliarsky M, Asthagiri A, Phillpot S R, Stachiotti M G and Migoni R L 2005 *Curr. Opin. Solid State Mater. Sci.* **9** 107–13
[18] Asthagiri A, Wu Z, Choudhury N and Cohen R E 2006 *Ferroelectrics* **333** 69–78
[19] Dick B G Jr and Overhauser A W 1958 *Phys. Rev.* **112** 90–103
[20] Ewald P P 1921 *Ann. Phys.* **64** 253–87
[21] Parry D E 1975 *Surf. Sci.* **49** 433–40
[22] Wolf D, Keblinski P, Phillpot S R and Eggebrecht J 1999 *J. Chem. Phys.* **110** 8254–82
[23] Tinte S, Stachiotti M G, Phillpot S R, Sepliarsky M, Wolf D and Migoni R L 2004 *J. Phys.: Condens. Matter* **16** 3495–506
[24] Shirane G, Axe J D, Harada J and Remeika J P 1970 *Phys. Rev.* B **2** 155–9
[25] Mabud S A and Glazer A M 1979 *J. Appl. Crystallogr.* **12** 49–53
[26] Burns G and Scott B A 1973 *Phys. Rev.* B **7** 3088–101
[27] Gavrilyachenko V G, Spinko R I, Martynenko M A and Fesenko E G 1970 *Sov. Phys.—Solid State* **12** 1203–4
[28] Ahart M, Asthagiri A, Ye Z G, Dera P, Mao H K, Cohen R E and Hemley R J 2007 *Phys. Rev.* B **75** 144410
[29] Vanderbilt D 1990 *Phys. Rev.* B **41** 7892–5
[30] King-Smith R D and Vanderbilt D 1994 *Phys. Rev.* B **49** 5828–44
[31] Padilla J and Vanderbilt D 1997 *Phys. Rev.* B **56** 1625–31
[32] Padilla J and Vanderbilt D 1998 *Surf. Sci.* **418** 64–70
[33] Monkhorst H J and Pack J D 1976 *Phys. Rev.* B **13** 5188–92
[34] Kresse G and Hafner J 1993 *Phys. Rev.* B **47** 558–61
[35] Kresse G and Furthmüller J 1996 *Phys. Rev.* B **54** 11169–86
[36] Kresse G and Furthmüller J 1996 *Comput. Mater. Sci.* **6** 15–50
[37] Henkelman G, Arnaldsson A and Jonsson H 2006 *Comput. Mater. Sci.* **36** 354–60
[38] Piskunov S, Kotomin E A, Heifets E, Maier J, Eglitis R I and Borstel G 2005 *Surf. Sci.* **575** 75–88
[39] Meyer B and Vanderbilt D 2001 *Phys. Rev.* B **63** 205426
[40] Sai N, Kolpak A M and Rappe A M 2005 *Phys. Rev.* B **72** 020101
[41] Kolpak A M, Sai N and Rappe A M 2006 *Phys. Rev.* B **74** 054112
[42] Neugebauer J and Scheffler M 1992 *Phys. Rev.* B **46** 16067–80
[43] Bengtsson L 1999 *Phys. Rev.* B **59** 12301–4
[44] Bickel N, Schmidt G, Heinz K and Müller K 1989 *Phys. Rev. Lett.* **62** 2009–11
[45] Meyer B, Padilla J and Vanderbilt D 1999 *Faraday Discuss.* **114** 395–405
[46] Meyer B and Vanderbilt D 2002 *Phys. Rev.* B **65** 104111
[47] Zhong W, King-Smith R D and Vanderbilt D 1994 *Phys. Rev. Lett.* **72** 3618–21
[48] Benson G C, Balk P and White P 1959 *J. Chem. Phys.* **31** 109–15
[49] Tang H, Bouju X, Joachim C, Girard C and Devillers J 1998 *J. Chem. Phys.* **108** 359–67
[50] Vogt J and Weiss H 2001 *Surf. Sci.* **491** 155–68
[51] Heifets E, Eglitis R I, Kotomin E A, Maier J and Borstel G 2001 *Phys. Rev.* B **64** 235417